

# Atomic Force Microscopy Reveals the Architecture of the Epithelial Sodium Channel (ENaC)<sup>5</sup>

Received for publication, June 23, 2011, and in revised form, July 18, 2011. Published, JBC Papers in Press, July 20, 2011, DOI 10.1074/jbc.M111.275289

Andrew P. Stewart<sup>†1</sup>, Silke Haerteis<sup>§2</sup>, Alexei Diakov<sup>§</sup>, Christoph Korbmayer<sup>§3</sup>, and J. Michael Edwardson<sup>†4</sup>

From the <sup>†</sup>Department of Pharmacology, University of Cambridge, Tennis Court Road, Cambridge CB2 1PD, United Kingdom and the <sup>§</sup>Institut für Zelluläre und Molekulare Physiologie, Friedrich-Alexander-Universität Erlangen-Nürnberg, Waldstrasse 6, 91054 Erlangen, Germany

The epithelial sodium channel (ENaC) is a member of the ENaC/degenerin superfamily. ENaC is a heteromultimer containing three homologous subunits ( $\alpha$ ,  $\beta$ , and  $\gamma$ ); however, the subunit stoichiometry is still controversial. Here, we addressed this issue using atomic force microscopy imaging of complexes between isolated ENaC and antibodies/Fab fragments directed against specific epitope tags on the  $\alpha$ -,  $\beta$ - and  $\gamma$ -subunits. We show that for  $\alpha$ -,  $\beta$ - and  $\gamma$ -ENaC alone, pairs of antibodies decorate the channel at an angle of 120°, indicating that the individual subunits assemble as homotrimers. A similar approach demonstrates that  $\alpha\beta\gamma$ -ENaC assembles as a heterotrimer containing one copy of each subunit. Intriguingly, all four subunit combinations also produce higher-order structures containing two or three individual trimers. The trimer-of-trimers organization would account for earlier reports that ENaC contains eight to nine subunits.

The epithelial sodium channel (ENaC)<sup>5</sup> is a member of the ENaC/degenerin superfamily, which also includes acid-sensing ion channels (ASICs; reviewed in Ref. 1). ENaC mediates Na<sup>+</sup> entry across the apical membranes of many absorptive epithelia, including the alveolar epithelium, salivary duct, distal colon, and sweat glands. ENaC plays a particularly important role in Na<sup>+</sup> transport across the aldosterone-sensitive distal nephron (reviewed in Ref. 2), which is responsible for the regulation of Na<sup>+</sup> and K<sup>+</sup> excretion, and thus plays an important role in the control of blood pressure. ENaC is the target of potassium-sparing diuretics such as amiloride and spironolactone used in the treatment of cardiovascular disease. Whereas amiloride is a direct blocker of the channel, the mineralocorticoid receptor

antagonist spironolactone inhibits ENaC activity by preventing its stimulation by aldosterone.

ENaC is a heteromultimer containing three homologous subunits ( $\alpha$ ,  $\beta$ , and  $\gamma$ ), which have 30–40% amino acid identity (3, 4). A fourth ENaC subunit,  $\delta$ -ENaC, has been cloned from a human kidney library (5). In heterologous expression systems,  $\delta$ -ENaC has functional similarities with  $\alpha$ -ENaC, but its physiological role is still unclear (6). Each ENaC subunit contains two transmembrane domains, a large extracellular loop, and short intracellular N and C termini. Full ENaC activity requires co-expression of all three subunits (4). In the past, it has been proposed that ENaC is assembled from either four (7–9) or eight to nine subunits (10, 11). However, the recently published crystal structure of ASIC 1a (12) suggests that ENaC is likely to be a trimer (13), although this has not been demonstrated.

We have developed a method, based on AFM imaging, for determining the stoichiometry and arrangement of subunits within multimeric proteins (reviewed in Ref. 14). The method involves engineering specific epitope tags onto each protein subunit and expressing the proteins exogenously in a suitable cell line (usually tsA 201). Membrane fractions from the transfected cells are solubilized in detergent, and the proteins are isolated by affinity chromatography using the epitope tags. The proteins are incubated with antibodies to the tags, and the resulting protein-antibody complexes are imaged by AFM. Proteins that have two bound antibodies are identified; the angles between the antibodies are measured and a frequency distribution of angles is produced. The properties of these distributions reveal the protein architecture. Previously, we have applied this method to the architecture of ionotropic neurotransmitter receptors, such as the P2X receptor (15), and ion channels, such as the TRPP2/TRPC1 channel (16). In the present study, we have used AFM imaging of channels decorated by antibodies against subunit-specific epitope tags to determine the subunit stoichiometry and architecture of ENaC.

## EXPERIMENTAL PROCEDURES

**Constructs**—cDNAs for human WT  $\alpha$ -,  $\beta$ -, and  $\gamma$ -ENaC, kindly provided by Harry Cuppens (Leuven, Belgium), were subcloned into the pcDNA3.1 vector. Linearized plasmids were used as templates for cRNA synthesis (mMessage mMachine, Ambion, Austin, Texas) using T7 as a promoter. Site-directed mutagenesis extension overlap PCR (QuikChange®, Stratagene, Amsterdam, Netherlands) was used to generate epitope-tagged ENaC subunit constructs. All constructs had an N-terminal HA epitope tag. In addition, the constructs had the

<sup>5</sup>The on-line version of this article (available at <http://www.jbc.org>) contains supplemental Figs. S1–S3.

<sup>1</sup>Member of the University of Cambridge MB/PhD Programme and supported by the Jean Shanks Foundation and the James Baird Fund.

<sup>2</sup>Supported by a young investigator grant from the IZKF (Interdisciplinary Centre of Clinical Research) and the Erlanger Leistungsbezogene Anschubfinanzierung und Nachwuchsfoerderung (ELAN) program of the Friedrich-Alexander-Universität Erlangen-Nürnberg and recipient of a travel grant from the Bayerische Forschungsförderung.

<sup>3</sup>Supported by the Deutsche Forschungsgemeinschaft (SFB 423, Project A12).

<sup>4</sup>Supported by Kidney Research UK. To whom correspondence should be addressed: Dept. of Pharmacology, University of Cambridge, Tennis Court Road, Cambridge CB2 1PD, United Kingdom. Tel.: 44-1223-334014; Fax: 44-1223-334100; E-mail: jme1000@cam.ac.uk.

<sup>5</sup>The abbreviations used are: ENaC, epithelial sodium channel; AFM, atomic force microscopy; ASIC, acid-sensing ion channel; NMDG, N-methyl-D-glucamine.

following C-terminal tags:  $\alpha$ -ENaC - V5 or FLAG;  $\beta$ -ENaC - V5 or His<sub>6</sub>; and  $\gamma$ -ENaC - V5. All tags were added directly to the ENaC sequence, except for  $\alpha$ HA/FLAG-ENaC, which had a short linker (AGGLAS) inserted between the ENaC sequence and the FLAG epitope. All constructs were subjected to sequence verification before use (GATC Biotech, Konstanz, Germany).

**Expression and Functional Analysis of ENaCs in *Xenopus laevis* Oocytes**—Oocyte experiments were performed essentially as described previously (6, 17). Oocytes were obtained from adult female *X. laevis* in accordance with the principles of German legislation, with approval by the animal welfare officer for the University of Erlangen-Nürnberg, and under the governance of the state veterinary health inspectorate (permit no. 621-2531.32-05/02). Animals were anesthetized in 0.2% MS222 and ovarian lobes were obtained through a small abdominal incision. Oocytes were isolated from the ovarian lobes by enzymatic digestion at 19 °C for 3–4 h with 600–700 units/ml type 2 collagenase from *Clostridium histolyticum* (CLS 2, Worthington, Lakewood, NJ) dissolved in a solution containing 82.5 mM NaCl, 2 mM KCl, 1 mM MgCl<sub>2</sub>, and 5 mM HEPES, pH 7.4. Defolliculated stage V–VI oocytes were injected (Nanoject II automatic injector, Drummond, Broomall, PA) with 0.2 ng cRNA (in RNase-free water) per ENaC subunit in a volume of 46 nl, unless stated otherwise. To minimize the risk of expression artifacts through differences in cRNA quality, cRNAs for WT and tagged ENaC were synthesized in parallel, and oocyte expression experiments were performed using at least two different batches of cRNA. Injected oocytes were stored at 19 °C in low sodium solution (87 mM *N*-methyl-D-glucamine (NMDG) chloride, 9 mM NaCl, 2 mM KCl, 1.8 mM CaCl<sub>2</sub>, 1 mM MgCl<sub>2</sub>, and 5 mM HEPES, pH 7.4) supplemented with 100 units/ml penicillin and 100  $\mu$ g/ml streptomycin.

Oocytes were routinely studied 2 days after injection. The two-electrode voltage-clamp technique used was essentially as described previously (6, 17). Individual oocytes were placed in a small experimental chamber and constantly superfused with high sodium solution ND96 (96 mM NaCl, 2 mM KCl, 1.8 mM CaCl<sub>2</sub>, 1 mM MgCl<sub>2</sub>, and 5 mM HEPES, pH 7.4) supplemented with amiloride (2  $\mu$ M). Oocytes were routinely clamped at a holding potential of –60 mV. Amiloride-sensitive ENaC-mediated whole-cell currents ( $\Delta I_{ami}$ ) were determined by washing out amiloride with amiloride-free ND96 and subtracting the whole-cell currents measured in the presence of amiloride from the corresponding whole-cell currents recorded in the absence of amiloride.

Single-channel recordings from outside-out membrane patches of ENaC expressing oocytes were performed essentially as described previously (17–20). Patch pipettes, pulled from borosilicate glass capillaries, had a tip diameter of 1–1.5  $\mu$ m after fire polishing. Pipettes were filled with potassium gluconate pipette solution (90 mM potassium gluconate, 5 mM NaCl, 2 mM Mg-ATP, 2 mM EGTA, and 10 mM HEPES, pH 7.28). Seals were formed in a low sodium NMDG chloride bath solution (95 mM NMDG chloride, 1 mM NaCl, 4 mM KCl, 1 mM MgCl<sub>2</sub>, 1 mM CaCl<sub>2</sub>, and 10 mM HEPES, pH 7.4). In this bath solution, a typical pipette resistance was 7 megohms. For the NaCl, KCl, and LiCl bath solutions, 95 mM NMDG chloride was replaced by 95 mM

NaCl, 95 mM KCl, or 95 mM LiCl, respectively. After seal formation, the bath solution was changed to the NaCl, LiCl, or KCl bath solutions. Membrane patches were voltage clamped at –70 mV, close to the calculated reversal potential of Cl<sup>–</sup> ( $E_{Cl} = -77.4$  mV) and K<sup>+</sup> ( $E_K = -79.4$  mV) under our experimental conditions. Experiments were performed at room temperature. Single-channel current data were initially filtered at 500 Hz and sampled at 2 kHz. In multichannel patches, current traces were refiltered at 50 Hz to resolve the single-channel current amplitude (*i*). *i* was derived from binned current amplitude histograms (18–21). The current level at which all channels are closed was determined in the presence of 2  $\mu$ M amiloride.

**Transient Transfection of tsA 201 Cells**—tsA 201 cells (a subclone of human embryonic kidney-293 cells stably expressing the SV40 large T-antigen) were grown in Dulbecco's modified Eagle's medium supplemented with 10% (v/v) fetal calf serum, 100 units/ml penicillin, and 100  $\mu$ g/ml streptomycin, in an atmosphere of 5% CO<sub>2</sub>/air. Transient transfections of tsA 201 cells with DNA were carried out using the CalPhos<sup>TM</sup> mammalian transfection kit (Clontech), according to the manufacturer's instructions. Protein expression and intracellular localization were checked using immunofluorescence analysis. Cells were fixed, permeabilized, and incubated with appropriate primary antibodies: mouse monoclonal anti-HA (Covance), mouse monoclonal anti-V5 (Invitrogen), mouse monoclonal anti-FLAG (Sigma), and rabbit polyclonal anti-His<sub>6</sub> (Research Diagnostics, Inc.), followed by Cy3-conjugated goat secondary antibodies (Sigma). Cells were imaged by confocal laser scanning microscopy.

**Solubilization and Isolation of Epitope-tagged ENaCs**—A total of 250  $\mu$ g of DNA was used to transfect cells in 5  $\times$  162 cm<sup>2</sup> culture flasks. When cells were triply transfected, equal amounts of DNA for each construct were used, up to a total of 250  $\mu$ g. After transfection, cells were incubated for 48 h to allow protein expression. Transfected cells were solubilized in 1% Triton X-100 for 1 h before centrifugation at 78,000  $\times$  g to remove insoluble material. To isolate ENaCs, the solubilized extract was incubated with either anti-HA- or anti-FLAG-agarose beads (Sigma) for 3 h. The beads were washed extensively, and bound proteins were eluted with HA or FLAG peptide (100  $\mu$ g/ml). In all cases, samples were analyzed by SDS-PAGE, and proteins were detected by immunoblotting with appropriate antibodies (see above).

**AFM Imaging**—Isolated proteins were diluted to a final concentration of 0.04 nM, and 45  $\mu$ l of the sample was allowed to adsorb to freshly cleaved, poly-L-lysine-coated mica disks. After a 5-min incubation, the sample was washed with BPC-grade water (Sigma) and dried under nitrogen. Imaging was performed with a Veeco Digital Instruments Multimode AFM controlled by a Nanoscope IIIa controller. Samples were imaged in air, using tapping mode. The silicon cantilevers used had a drive frequency of  $\sim$ 300 kHz and a specified spring constant of 40 Newtons/meter (Olympus). The applied imaging force was kept as low as possible ( $A_s/A_0 \sim 0.85$ ).

The molecular volumes of the protein particles were determined from particle dimensions based on AFM images. After adsorption of the proteins onto the mica support, the particles adopted the shape of a spherical cap. As described previously

## Architecture of ENaC

(22), the heights and radii were measured from multiple cross-sections of the same particle, and the molecular volume was calculated using Equation 1,

$$V_m = (\pi h/6)(3r^2 + h^2) \quad (\text{Eq. 1})$$

where  $h$  is the particle height, and  $r$  is the radius. Molecular volume based on molecular mass was calculated using Equation 2,

$$V_c = (M_0/N_0)(V_1 + dV_2) \quad (\text{Eq. 2})$$

where  $M_0$  is the molecular mass,  $N_0$  is Avogadro's number,  $V_1$  and  $V_2$  are the partial specific volumes of particle ( $0.74 \text{ cm}^3/\text{g}$ ) and water ( $1 \text{ cm}^3/\text{g}$ ), respectively, and  $d$  is the extent of protein hydration (taken as  $0.4 \text{ g water/g protein}$ ).

Note that it has been shown previously (22) that the molecular volumes of proteins measured by imaging in air are very similar to the values obtained by imaging under fluid; hence, the process of drying does not significantly affect the measured molecular volume. It has also been shown by us (23) and by others (22) that there is a close correspondence between the measured and predicted molecular volumes for various proteins over a wide range of molecular masses; hence, molecular volume is accurately measured by AFM imaging.

**Selection of Binding Events**—Several criteria were used to identify ENaC-antibody complexes. Heights and radii were measured for all particles, and the particle volumes were calculated. Bound particles needed to have between half and twice the predicted volume of  $285 \text{ nm}^3$  to be accepted as antibodies. For samples containing both antibodies and Fab fragments, the same criterion was used but with a volume range of  $190\text{--}570 \text{ nm}^3$  for antibodies and  $47.5\text{--}170 \text{ nm}^3$  for Fab fragments. These reduced ranges were applied to minimize confusion between antibodies and Fabs. A cross-section was drawn through the junction between the antibody and the adjacent ENaC, and the height of the lowest point between antibody and ENaC was measured. This height needed to be  $>0.3 \text{ nm}$  for the antibody to be considered bound. Any particle was rejected if its length was greater than twice its width. To be considered a double binding event, all particles and both binding events needed to meet all of the above criteria.

**Statistical Analysis**—For the experiments with *Xenopus laevis* oocytes, data are presented as means  $\pm$  S.E.  $N$  indicates the number of different batches of oocytes, and  $n$  represents the number of individual oocytes studied. Statistical significance was assessed by an appropriate version of Student's  $t$  test with GraphPad Prism for Windows (version 4.03, GraphPad Software, Inc.).

Histograms of AFM data were drawn with bin widths chosen according to Scott's equation (Equation 3),

$$\text{Bin width} = 3.5\sigma/n^{1/3} \quad (\text{Eq. 3})$$

where  $\sigma$  is an estimate of S.D., and  $n$  is the sample size (24). Where Gaussian curves were fitted to the data, the number of curves was chosen so as to maximize the  $r^2$  value, while giving significantly different means using Welch's  $t$  test for unequal sample sizes and unequal variances (25).

## RESULTS

In addition to WT ENaC subunits, five epitope-tagged subunits were used in this study:  $\alpha\text{HA}/\text{V5}$ ,  $\beta\text{HA}/\text{V5}$ ,  $\gamma\text{HA}/\text{V5}$ ,  $\alpha\text{HA}/\text{FLAG}$ , and  $\beta\text{HA}/\text{His}_6$ . To demonstrate that the tagged ENaC subunits used in our experiments are functional, we tested them using the *X. laevis* oocyte expression system. Fig. 1A shows representative whole-cell current traces from oocytes expressing either  $\alpha\beta\gamma$ -ENaC (WT, *left*) or  $\alpha\text{HA}/\text{FLAG}$ -,  $\beta\text{HA}/\text{His}_6$ -, and  $\gamma\text{HA}/\text{V5}$ -ENaC (3xTag, *right*). As illustrated by these traces, and summarized in Fig. 1B, robust amiloride-sensitive currents were detectable with all combinations of tagged or untagged ENaC subunits, demonstrating that the tags do not abolish ENaC function. However, ENaC currents were significantly reduced (relative to WT) in oocytes expressing triple-tagged ENaC and also in oocytes expressing  $\gamma\text{HA}/\text{V5}$ -ENaC together with WT  $\alpha$ - and  $\beta$ -ENaC (Fig. 1B). Immunoblot analysis (supplemental Fig. S1) confirmed expression of all three tagged subunits with the expected cleavage products (6) albeit with slightly reduced overall protein expression levels for the tagged  $\beta$ - and  $\gamma$ -subunits. Thus, the reduced current levels observed with triple-tagged ENaC may be caused by subtle effects of the tags on translation efficiency and/or on channel trafficking to the plasma membrane.

To investigate a possible effect of the tags on the single-channel properties of ENaC, we performed patch clamp experiments as described previously (17–19). Outside-out patches were obtained from oocytes expressing  $\alpha\text{HA}/\text{FLAG}$ -,  $\beta\text{HA}/\text{His}_6$ -, and  $\gamma\text{HA}/\text{V5}$ -ENaC. Fig. 1C shows typical single-channel current traces recorded at different holding potentials ( $V_{\text{hold}}$ ). Corresponding  $I/V$  plots (Fig. 1D) indicate that the triple-tagged channel has a single-channel conductance ( $5.2 \text{ pS}$ ) that is typical for WT human ENaC (17, 26). We also investigated the ion selectivity of the triple-tagged channel. As illustrated in the representative trace (Fig. 1E), the single-channel current amplitude increased from  $-0.32 \text{ pA}$  to  $-0.56 \text{ pA}$  upon changing the bath solution from  $\text{Na}^+$  to  $\text{Li}^+$ . In similar experiments, the single-channel currents averaged  $-0.34 \pm 0.02$  (S.E.) pA ( $n = 5$ ) in  $\text{Na}^+$  and  $-0.61 \pm 0.02$  pA ( $n = 5$ ) in  $\text{Li}^+$ , which is consistent with the well-known finding that the single-channel  $\text{Li}^+$  conductance of ENaC is about twice its  $\text{Na}^+$  conductance. No single-channel events were detected at  $V_{\text{hold}} = -70 \text{ mV}$  with  $\text{K}^+$  in the bath solution, indicating that, as with WT ENaC, the triple-tagged channel is not permeable to  $\text{K}^+$ . Taken together, our findings indicate that the tags do not affect the single-channel conductance or ion selectivity of ENaC.

tsA 201 cells were singly transfected with DNA encoding HA/V5-tagged  $\alpha$ -,  $\beta$ -, or  $\gamma$ -ENaC. Protein expression was confirmed by immunofluorescence, using anti-HA and anti-V5 antibodies. The staining patterns showed the expression of all three subunits (Fig. 2A). In contrast, use of an anti-Myc antibody as a negative control produced only background immunofluorescence signals (data not shown). Brightfield imaging revealed that in all cases the tsA 201 cells were confluent (data not shown); hence, the transfection efficiency was 20–30%. Cells singly-transfected with  $\alpha\text{HA}/\text{FLAG}$ -ENaC,  $\beta\text{HA}/\text{His}_6$ -ENaC, or  $\gamma\text{HA}/\text{V5}$ -ENaC also gave positive immunofluorescence signals with anti-FLAG, anti- $\text{His}_6$ , and anti-V5 antibod-

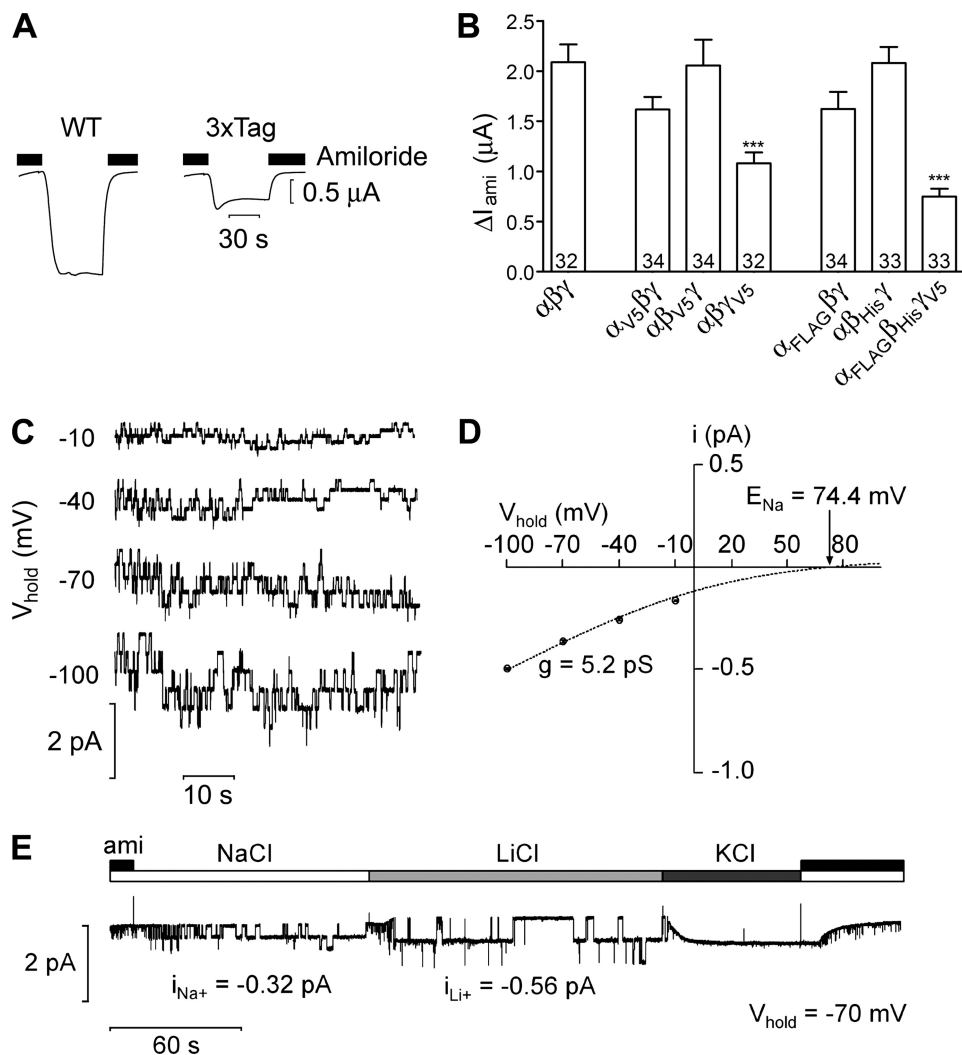


**FIGURE 1. Epitope-tagged ENaCs are functional.** *A*, representative whole-cell current traces from *X. laevis* oocytes expressing either wild type  $\alpha\beta\gamma$ -ENaC (WT; left) or  $\alpha$ HA/FLAG-ENaC,  $\beta$ HA/His<sub>6</sub>-ENaC, and  $\gamma$ HA/V5-ENaC (3xTag; right), at a holding potential of  $-60$  mV. Amiloride ( $2 \mu M$ ) was present in the bath to specifically inhibit ENaC as indicated by the black bars. Washout of amiloride revealed an inward current corresponding to the ENaC-mediated sodium current; reapplication of amiloride returned the whole-cell current toward the initial baseline level. *B*, summary of results of experiments obtained from oocytes expressing various combinations of tagged and untagged ENaC subunits. Only the C-terminal tag is indicated; all constructs also had an N-terminal HA tag. Numbers inside of the columns indicate the number of individual oocytes measured. Four different batches of oocytes were used. \*\*\*,  $p < 0.001$ , unpaired *t* test. *C*, representative single-channel current traces at different holding potentials ( $V_{hold}$ ) from an outside-out patch of an oocyte expressing  $\alpha$ HA/FLAG-,  $\beta$ HA/His<sub>6</sub>-, and  $\gamma$ HA/V5-ENaC. The current level at which all channels are closed was determined in the presence of amiloride ( $2 \mu M$ ). *D*, average single-channel *I/V* plots calculated from recordings (four patches from two batches of oocytes) similar to those shown in (*C*). Binned current amplitude histograms (not shown for clarity) were used to determine the single-channel current amplitude (*i*) at each holding potential. The dashed line represents a Goldman-Hodgkin-Katz fit of the data for a Na<sup>+</sup>-selective channel with a predicted Na<sup>+</sup> equilibrium potential ( $E_{Na^+}$ ) of  $74.4$  mV. Single-channel conductance (*g*) was calculated from the fit of the average *I/V* plots. *E*, representative single-channel current recording obtained at  $V_{hold} = -70$  mV from an outside-out patch from an oocyte expressing  $\alpha$ HA/FLAG-ENaC,  $\beta$ HA/His<sub>6</sub>-ENaC, and  $\gamma$ HA/V5-ENaC. Amiloride (*ami*;  $2 \mu M$ ), NaCl, KCl, or LiCl were present in the bath solution as indicated by the bars. The single-channel current amplitudes for Na<sup>+</sup> and Li<sup>+</sup> ( $i_{Na^+}$  and  $i_{Li^+}$ , respectively) were determined as described in *D*. Note that no single-channel events were detected in the presence of KCl in the bath.

ies, respectively (Fig. 2*B*). The reticular staining patterns suggest that all tagged ENaC subunits were localized predominantly in the endoplasmic reticulum.

Cells expressing HA/V5-tagged  $\alpha$ -,  $\beta$ -, or  $\gamma$ -ENaC were solubilized in 1% Triton X-100, and proteins were isolated through the binding of the HA tags to anti-HA-agarose beads, followed by elution with the HA peptide. Isolated proteins were immunoblotted with an anti-HA antibody. In fractions from cells expressing HA/V5-tagged  $\alpha$ -,  $\beta$ -, or  $\gamma$ -ENaC, the antibody labeled major bands at 90/85, 95, or 90/85 kDa, respectively, consistent with the expected sizes of the ENaC subunits, with their epitope tags (Fig. 2*C*). Proteins were also isolated from a

Triton X-100-solubilized membrane fraction of cells triply transfected with DNA encoding  $\alpha$ HA/FLAG-ENaC,  $\beta$ HA/His<sub>6</sub>-ENaC, and  $\gamma$ HA/V5-ENaC via the FLAG tag on  $\alpha$ -ENaC. On immunoblots of the isolated protein sample, anti-FLAG, anti-His<sub>6</sub>, and anti-V5 antibodies again labeled major bands at 90/85, 95, and 90/85 kDa, respectively (Fig. 2*D*). A smaller band, at  $\sim 18$  kDa was also detected by the anti-V5 antibody; this is likely a cleavage product of  $\gamma$ HA/V5-ENaC (27). Hence, the anti-FLAG-agarose successfully captured the appropriate proteins from the transfected cells. This result also demonstrates that ENaC subunit-subunit interactions persist throughout the purification procedure.

## Architecture of ENaC

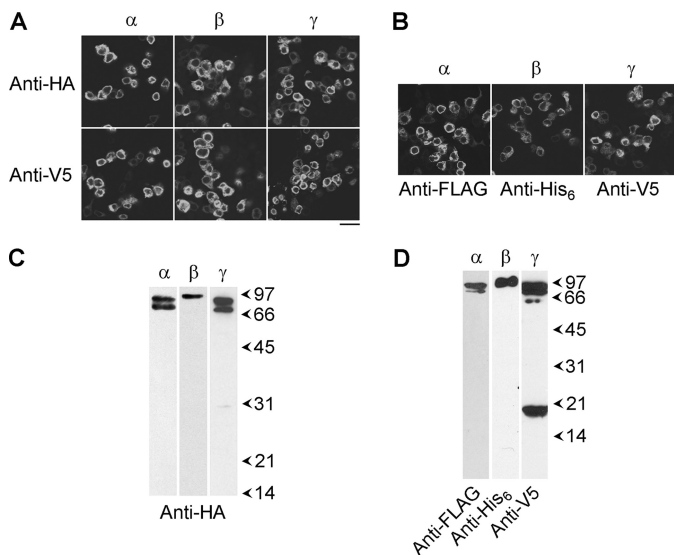


**FIGURE 2. Expression of ENaCs and isolation from tsA 201 cells.** *A*, cells were transiently transfected with DNA encoding HA/V5-tagged  $\alpha$ -,  $\beta$ -, or  $\gamma$ -ENaC. Cells were fixed, permeabilized, and incubated with either mouse monoclonal anti-HA or mouse monoclonal anti-V5 antibodies, followed by Cy3-conjugated goat anti-mouse secondary antibody. Cells were imaged by confocal laser scanning microscopy. Scale bar, 50  $\mu$ m. *B*, cells were singly transfected with  $\alpha$ HA/FLAG-ENaC,  $\beta$ HA/His<sub>6</sub>-ENaC, or  $\gamma$ HA/V5-ENaC. Cells were fixed, permeabilized, and incubated with mouse monoclonal anti-FLAG, rabbit polyclonal anti-His<sub>6</sub>, or mouse monoclonal anti-V5 antibodies, as appropriate, followed by Cy3-conjugated goat secondary antibodies. *C*, detection of HA/V5-tagged  $\alpha$ -,  $\beta$ -, and  $\gamma$ -ENaC in samples isolated from singly transfected cells by anti-HA affinity chromatography. Samples were analyzed by SDS-PAGE and immunoblotting using an anti-HA antibody, followed by horseradish peroxidase-conjugated goat secondary antibodies, with enhanced chemiluminescence detection. Arrowheads indicate molecular mass markers (kDa). *D*, detection of  $\alpha$ HA/FLAG-ENaC,  $\beta$ HA/His<sub>6</sub>-ENaC, and  $\gamma$ HA/V5-ENaC in samples isolated from triply transfected cells by anti-FLAG affinity chromatography.  $\alpha$ -,  $\beta$ -, and  $\gamma$ -ENaC were visualized using anti-FLAG, anti-His<sub>6</sub>, and anti-V5 antibodies, respectively.

Proteins isolated from cells that had been singly transfected with DNA encoding HA/V5-tagged  $\alpha$ -,  $\beta$ -, or  $\gamma$ -ENaC were imaged by AFM. A representative low magnification AFM image of an  $\alpha$ -ENaC sample reveals a heterogeneous distribution of particles (Fig. 3A).  $\alpha$ -ENaC was incubated with an anti-V5 antibody (of the immunoglobulin G class), which should decorate the C-terminal V5 epitope tag present on each subunit. A low magnification AFM image of  $\alpha$ -ENaC-antibody complexes is shown in Fig. 3B. Several particles can be seen to be decorated by either one (Fig. 3B, arrowheads) or two (Fig. 3B, arrows) accessory particles. The accessory particles had a molecular volume of  $\sim 250$  nm<sup>3</sup>, close to the expected volume of 285 nm<sup>3</sup> for an immunoglobulin G molecule, with a molecular mass of 150 kDa. Thus, these particles represent anti-V5 antibodies bound to the V5 epitope on  $\alpha$ -ENaC. Similar results were obtained for both  $\beta$ - and  $\gamma$ -ENaC (supplemental Fig. S2). The numbers of double binding events per AFM image with the anti-V5 antibody were 0.82 for  $\alpha$ -ENaC ( $n = 165$  images), 0.36 for  $\beta$ -ENaC ( $n = 298$  images), and 0.51 for  $\gamma$ -ENaC ( $n = 276$  images). In contrast, corresponding values for double decoration events per image for a negative control antibody, anti-Myc, were 0.12 for  $\alpha$ -ENaC ( $n = 102$  images), 0.03 for  $\beta$ -ENaC ( $n = 98$  images), and 0.06 for  $\gamma$ -ENaC ( $n = 107$  images). Given that all images had comparable particle densities, these data confirm that the vast majority of the double binding events seen with

anti-V5 antibody were specific. A gallery of doubly decorated particles for  $\alpha$ -,  $\beta$ -, and  $\gamma$ -ENaC is shown in Fig. 3C. Frequency distributions of molecular volumes of particles decorated by two antibodies were produced for each subunit (Fig. 3, D–F). Each distribution had three prominent molecular volume peaks. For  $\alpha$ -ENaC, the peaks were at  $485 \pm 19$  nm<sup>3</sup> ( $n = 76$ ),  $910 \pm 21$  nm<sup>3</sup> ( $n = 42$ ), and  $1374 \pm 81$  nm<sup>3</sup> ( $n = 18$ ; Fig. 3D). For  $\beta$ -ENaC, the peaks were at  $497 \pm 24$  nm<sup>3</sup> ( $n = 63$ ),  $908 \pm 14$  nm<sup>3</sup> ( $n = 14$ ), and  $1405 \pm 92$  nm<sup>3</sup> ( $n = 29$ ; Fig. 3E); and for  $\gamma$ -ENaC, the peaks were at  $460 \pm 16$  nm<sup>3</sup> ( $n = 78$ ),  $911 \pm 30$  nm<sup>3</sup> ( $n = 35$ ), and  $1441 \pm 69$  nm<sup>3</sup> ( $n = 28$ ; Fig. 3F). Note that the antibody-decorated particles shown in Fig. 3C are from the lowest volume peaks in Fig. 3, D–F. The molecular volume predicted for an ENaC subunit, on the basis of a molecular mass of  $\sim 95$  kDa, is 180 nm<sup>3</sup>; hence, an  $\alpha$ -ENaC homotrimer would have a predicted molecular volume of 540 nm<sup>3</sup>. The lowest measured volumes for all three subunits are therefore consistent with a trimeric structure. The two higher volumes are approximately double and triple the lower volume, suggesting that they might represent dimers- and trimers-of-trimers.

We identified  $\alpha$ -,  $\beta$ -, and  $\gamma$ -ENaC homomers that had been decorated by two antibodies and measured the angles between the bound antibodies. This was done in each case by joining the highest point on the central particle (the ENaC homomer) to the highest points on the peripheral particles (the antibodies) by lines and then determining the angle between the two lines. The frequency distributions of angles obtained are shown in Fig. 3, G–I. The angle distributions each had a single peak at  $110 \pm 2^\circ$  ( $n = 76$ ) for  $\alpha$ -ENaC (Fig. 3G),  $116 \pm 3^\circ$  ( $n = 63$ ) for  $\beta$ -ENaC (Fig. 3H), and  $123 \pm 2^\circ$  ( $n = 78$ ) for  $\gamma$ -ENaC (Fig. 3I). All three angle peaks are close to the  $120^\circ$  angle expected for a homotrimer.

$\alpha\beta\gamma$ -ENaC was isolated from detergent extracts of cells that had been triple-transfected with  $\alpha$ HA/FLAG-ENaC,  $\beta$ HA/His<sub>6</sub>-ENaC, and  $\gamma$ HA/V5-ENaC through the binding of the FLAG tag on  $\alpha$ -ENaC to anti-FLAG-agarose beads. As described above (Fig. 2D), immunoblotting revealed the presence of all three subunits in the isolated protein sample. AFM imaging of the ENaC sample (Fig. 4A) revealed a heterogeneous distribution of particles, as for the homomers. The isolated ENaC particles must contain  $\alpha$ -ENaC because that is the subunit that contains the FLAG tag used to purify the protein. To detect the presence of  $\beta$ - and  $\gamma$ -ENaC, we used anti-His<sub>6</sub> antibodies and anti-V5 Fab fragments, respectively. These two ligands are easily distinguishable by AFM on the basis of size (see supplemental Fig. S3). A low-magnification image of ENaCs that had been incubated with anti-His<sub>6</sub> antibody and anti-V5 Fab fragments is shown in Fig. 4B. Particles can be seen that are decorated by either a single antibody (Fig. 4B, arrowhead), a single Fab fragment (Fig. 4B, arrow), or both an antibody and a Fab fragment (circled). As for the ENaC homomers, a frequency distribution of molecular volumes of particles decorated by an antibody and a Fab fragment had three prominent peaks (Fig. 4C), at  $472 \pm 11$  nm<sup>3</sup> ( $n = 42$ ),  $868 \pm 27$  nm<sup>3</sup> ( $n = 44$ ), and  $1539 \pm 69$  nm<sup>3</sup> ( $n = 36$ ). The lowest volume is close to the predicted molecular volume for an ENaC trimer (540 nm<sup>3</sup>), and the higher volumes are approximately twice and three times this volume, suggesting that the  $\alpha\beta\gamma$ -ENaC, like the

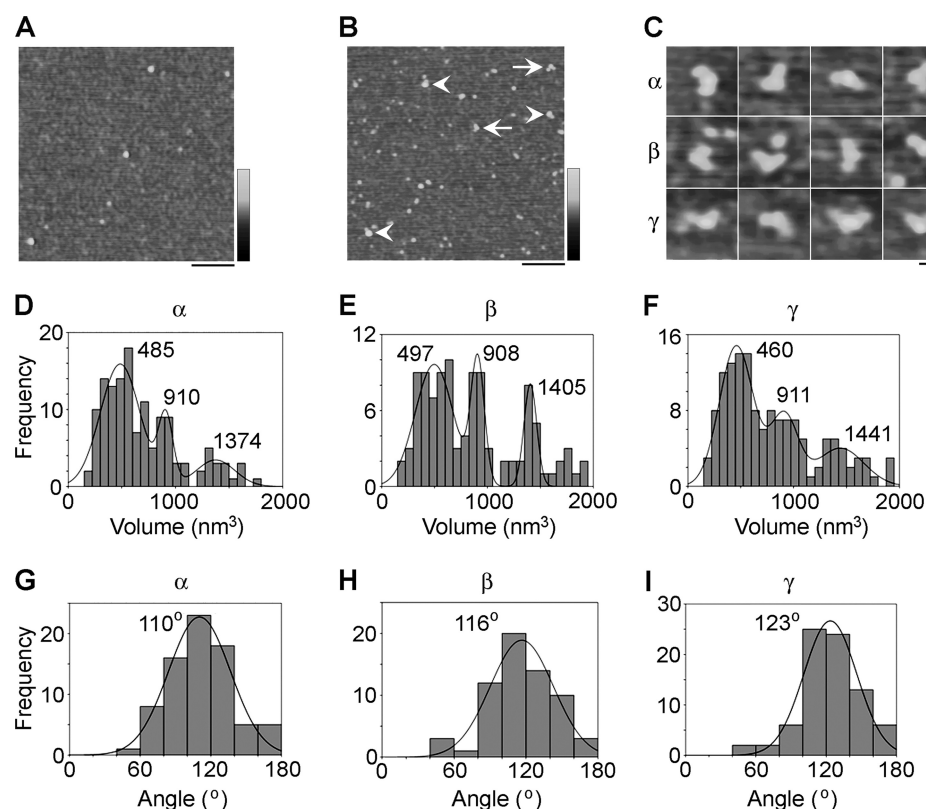


**FIGURE 3. Determination of the assembly state of ENaC homomers.** *A*, low magnification AFM image of  $\alpha$ HA/V5-ENaC. Note that the sample contains particles of various sizes. *Scale bar*, 200 nm; *shade-height scale*, 0–4 nm. *B*, low magnification image of  $\alpha$ HA/V5-ENaC that had been incubated with anti-V5 antibodies. *Arrowheads* indicate singly decorated particles; *arrows* indicate doubly decorated particles. *Scale bar*, 200 nm; *shade-height scale*, 0–4 nm. *C*, gallery of zoomed images of  $\alpha$ HA/V5-ENaC (*top*),  $\beta$ HA/V5-ENaC (*middle*), and  $\gamma$ HA/V5-ENaC (*bottom*) particles that are decorated by two peripheral particles (anti-V5 antibodies). *Scale bar*, 50 nm; *shade-height scale*, 0–2.5 nm. *D–F*, frequency distributions of molecular volumes of  $\alpha$ HA/V5-ENaC (*D*),  $\beta$ HA/V5-ENaC (*E*), and  $\gamma$ HA/V5-ENaC (*F*) particles that were decorated by two anti-V5 antibodies. The *curves* indicate the fitted Gaussian functions. The means of the distributions are indicated. Note that the antibody-decorated particles shown in *C* are from the lowest volume peaks in *D–F*. *G–I*, frequency distributions of angles between pairs of anti-V5 antibodies bound to  $\alpha$ HA/V5-ENaC (*G*),  $\beta$ HA/V5-ENaC (*H*), and  $\gamma$ HA/V5-ENaC (*I*). The *curves* indicate the fitted Gaussian functions. The peaks of the distributions are indicated.

ENaC homomers, assembles as a trimer and also as dimers- and trimers-of-trimers.

Fig. 4*D* shows a gallery of ENaC particles that are decorated by both an anti-His<sub>6</sub> antibody and an anti-V5 Fab fragment. Two arrangements of antibody/Fab pairs were seen, one in the order antibody-Fab (clockwise; *top panels*) and one in the order Fab-antibody (*bottom panels*). Approximately equal numbers of these two arrangements were seen. This result could indicate either a random assembly of subunits around the channel pore or (probably more likely) a random attachment of channels to the mica substrate (*i.e.* extracellular or intracellular face down). In fact, a recent report (28) has suggested an  $\alpha\gamma\beta$  arrangement (clockwise when viewed from the outside of the cell), although this study began with the assumption that ENaC assembled in the same way as ASIC1a, that is, as a trimer. A schematic diagram of the alternative antibody/Fab decoration profiles is shown in Fig. 4*E*. A frequency distribution of angles between bound antibody/Fab pairs (Fig. 4*F*) had a single peak at  $122 \pm 2^\circ$  ( $n = 42$ ), close to the expected value of  $120^\circ$  for an ENaC trimer.

The observation of three molecular volume peaks for doubly decorated ENaCs suggests that the individual trimers might assemble to form higher-order structures. The presence of these structures might account for the heterogeneity observed in AFM images of ENaC alone. In fact, it is possible to assign

particles in low magnification images of  $\alpha\beta\gamma$ -ENaC heteromers into one of the three molecular volume peaks, as shown in Fig. 5*A*. Intriguingly, for all combinations of subunits (*i.e.*  $\alpha$ -,  $\beta$ -,  $\gamma$ -, and  $\alpha\beta\gamma$ -ENaC), we observed examples of triplets of identical particles, with a combined molecular volume that falls within the highest volume peak. An example of such a triplet is indicated in Fig. 5*A* by the *arrow*, and a gallery of such particles for  $\alpha$ -,  $\beta$ -,  $\gamma$ -, and  $\alpha\beta\gamma$ -ENaC is shown in Fig. 5*B*. We suggest that these triplets are trimers-of-trimers that have settled onto the mica substrate and then fallen apart into individual trimers. Similar structures have been seen previously in our analysis of the structure of ASIC1a, which is also known to assemble as a trimer (29, 30).

We next examined the antibody decoration profile of the higher-order structures. Following incubation of  $\alpha\beta\gamma$ -ENaC with either anti-His<sub>6</sub> or anti-V5 antibodies (without Fab fragments), we saw antibody-decorated particles. Fig. 5*C* shows low magnification images of  $\alpha\beta\gamma$ -ENaC decorated with either anti-His<sub>6</sub> (*left panel*) or anti-V5 (*right panel*) antibodies. In Fig. 5*C*, singly and doubly decorated particles are indicated by *arrowheads* and *arrows*, respectively. The numbers of double binding events per AFM image with the anti-His<sub>6</sub> and anti-V5 antibodies were 0.26 ( $n = 216$  images) and 0.17 ( $n = 264$  images), respectively. In contrast, corresponding values for double dec-

## Architecture of ENaC

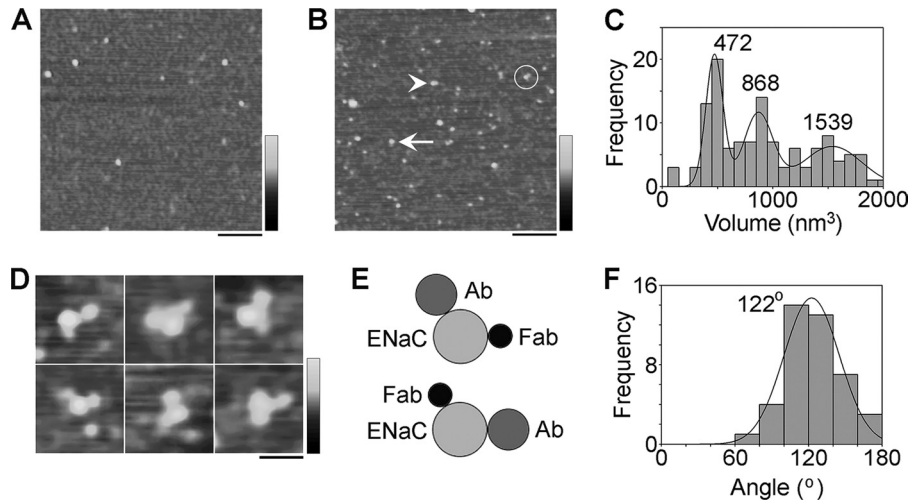


**FIGURE 4. Determination of the assembly state of ENaC heteromers.** *A*, low magnification image of proteins isolated from cells expressing  $\alpha$ HA/FLAG-ENaC,  $\beta$ HA/His<sub>6</sub>-ENaC, and  $\gamma$ HA/V5-ENaC. Note that the sample contains particles of various sizes. Scale bar, 200 nm; shade-height scale, 0–4 nm. *B*, low magnification image of a sample of isolated  $\alpha\beta\gamma$ -ENaC that had been incubated with anti-His<sub>6</sub> antibodies and anti-V5 Fab fragments. The arrowhead indicates an ENaC particle that is singly decorated by an anti-His<sub>6</sub> antibody; the arrow indicates an ENaC particle that is singly decorated by an anti-V5 Fab fragment; an ENaC particle that is decorated by both an anti-His<sub>6</sub> antibody and an anti-V5 Fab fragment is circled. Scale bar, 200 nm; shade-height scale, 0–4 nm. *C*, frequency distribution of molecular volumes of ENaC particles that were decorated by both an anti-His<sub>6</sub> antibody and an anti-V5 Fab fragment. The curves indicate the fitted Gaussian functions. The means of the distribution are indicated. *D*, gallery of zoomed images of ENaC particles from the lowest volume peak in (*C*) that are decorated by both an anti-His<sub>6</sub> antibody and an anti-V5 Fab fragment. Scale bar, 50 nm; shade-height scale, 0–2.5 nm. *E*, schematic illustration of the alternative antibody/Fab decoration patterns seen in *D*. *F*, frequency distribution of angles between bound anti-His<sub>6</sub> antibodies and anti-V5 Fab fragments. The curve indicates the fitted Gaussian function. The peak of the distribution is indicated.

oration events per image for a negative control antibody, anti-Myc, in the same experiments were 0.04 ( $n = 108$  images) and 0.02 ( $n = 92$  images), respectively. Hence, as for the ENaC homomers (above), the vast majority of the double binding events seen with anti-His<sub>6</sub> and anti-V5 antibodies were specific. A gallery of doubly decorated  $\alpha$ -,  $\beta$ -,  $\gamma$ -, and  $\alpha\beta\gamma$ -ENaC particles is shown in Fig. 5*D*. Frequency distributions of molecular volumes of  $\alpha\beta\gamma$ -ENaC particles decorated by two anti-His<sub>6</sub> (Fig. 5*E*) or anti-V5 (Fig. 5*F*) antibodies both had two prominent molecular volume peaks, at  $939 \pm 49 \text{ nm}^3$  ( $n = 31$ ) and  $1573 \pm 25 \text{ nm}^3$  ( $n = 26$ ) for anti-His<sub>6</sub> and at  $959 \pm 35 \text{ nm}^3$  ( $n = 27$ ) and  $1459 \pm 19 \text{ nm}^3$  ( $n = 19$ ) for anti-V5. Significantly, the lowest volume peak at  $\sim 480 \text{ nm}^3$  seen for antibody/Fab double decoration of  $\alpha\beta\gamma$ -ENaC and for anti-V5 double decoration of all three ENaC homomers was absent. As discussed above, the two higher volumes likely represent dimers- and trimers-of-trimers. The fact that the individual trimers cannot be doubly decorated by either antibody indicates that the vast majority of ENaC trimers produced in cells expressing all three subunits contain one copy of each subunit, ruling out the possibility that substantial populations of  $\alpha\beta\beta$ - and  $\alpha\gamma\gamma$ -ENaCs exist.

## DISCUSSION

In this study, we have shown that  $\alpha\beta\gamma$ -ENaC assembles as a heterotrimer, that  $\alpha$ -,  $\beta$ -, and  $\gamma$ -ENaC can each form homotrimers, and that ENaC trimers interact to form dimers- and trimers-of-trimers. Trimeric assembly of ENaC is consistent with the crystal structure of ASIC1a, another member of the ENaC/degenerin superfamily (12) and with the results of a subsequent AFM study on ASIC1a (29). Assembly into trimers-of-trimers also accounts for previous reports of a very large ENaC complex with eight to nine subunits. One of these previous studies involved testing the functional properties of ENaCs

containing mixed WT and mutant  $\gamma$ -subunits and examining the migration of the channel on sucrose density gradients (10). Another involved analysis of the sizes of intramembranous particles visualized by freeze fracture followed by electron microscopy (11). Notably, a trimer-of-trimers structure would also explain coimmunoprecipitation and FRET data, showing that ENaC contains at least two copies of each subunit (31). Evidence for the functional relevance of a ‘triple-barrel’ organization of ENaC has also been presented, indicating that the trimer-of-trimers structure reported here might be physiologically relevant (32).

Trimer-of-trimers assembly, while consolidating the numerous reports of a larger structure with both the crystallography and AFM data on ASIC1a, conflicts with the results of a number of previous studies, which have reported that ENaC assembles as a tetramer. In one of these studies (7), analysis of expression of  $\alpha$ -,  $\beta$ - and  $\gamma$ -ENaC at the surface of *Xenopus* oocytes showed that the  $\alpha$ -subunit was the most abundant, when normalized to the sodium current. In addition, functional assays based on the sensitivities of channels bearing mutations in individual subunits to inhibitors such as Zn<sup>2+</sup> and amiloride suggested a stoichiometry of  $\alpha_2\beta\gamma$ . Finally, expression of a variety of concatenated subunits suggested that the functional channel consists of two copies of  $\alpha$ -ENaC separated by  $\beta$ - and  $\gamma$ -ENaC. Another study (9) exploited mutations in the three subunits that were known to alter single-channel conductances. When the three WT subunits were expressed in the oocytes along with an equimolar amount of the mutant  $\alpha$ -subunit, a novel intermediate conductance state was seen, which was interpreted as arising from channels containing one WT and one mutant  $\alpha$ -subunit. In contrast, no intermediate conductance states were seen when the mutant  $\beta$ - and  $\gamma$ -subunits were used. These data

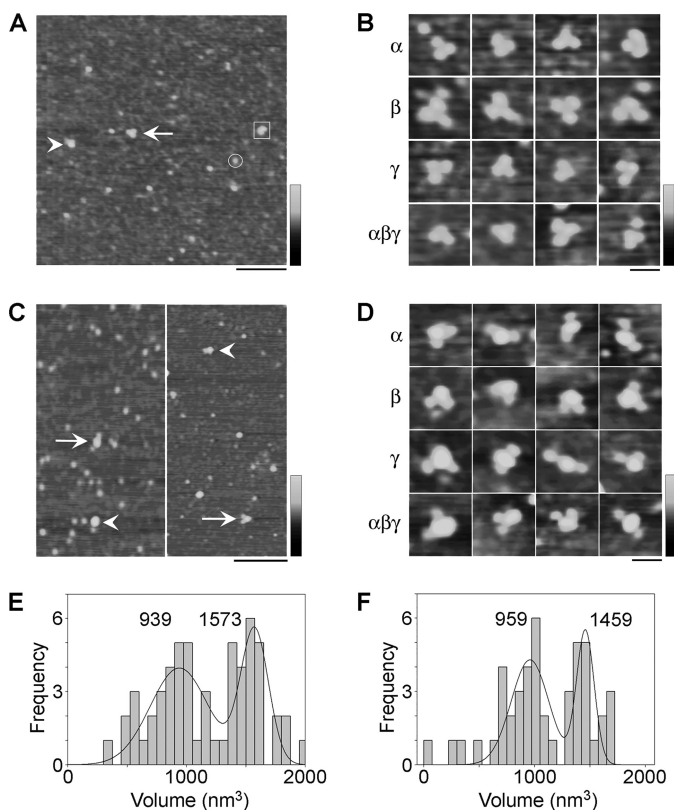


**FIGURE 5. Analysis of the higher-order structure of ENaC.** A, low magnification image of proteins isolated from cells expressing  $\alpha$ HA/FLAG-ENaC,  $\beta$ HA/His<sub>6</sub>-ENaC, and  $\gamma$ HA/V5-ENaC. Representative particles belonging to each of the three volume peaks in Fig. 4C are indicated as follows: *circle*, peak 1; *box*, peak 2; *arrowhead*, peak 3. The *arrow* indicates a triple particle. Scale bar, 200 nm; shade-height scale, 0–4 nm. B, gallery of zoomed images of triple particles isolated from cells expressing  $\alpha$ -,  $\beta$ -,  $\gamma$ -, or  $\alpha\beta\gamma$ -ENaC. Scale bar, 50 nm; shade-height scale, 0–2.5 nm. C, low magnification images of samples of isolated  $\alpha\beta\gamma$ -ENaC that had been incubated with either anti-His<sub>6</sub> (left panel) or anti-V5 antibodies (right panel). Arrowheads indicate singly decorated ENaC particles; arrows indicate doubly decorated particles. Scale bar, 200 nm; shade-height scale, 0–4 nm. D, gallery of zoomed images of ENaC particles from volume peaks 2 and 3, isolated from cells expressing  $\alpha$ -,  $\beta$ -,  $\gamma$ -, or  $\alpha\beta\gamma$ -ENaC, that are decorated by two antibodies. Scale bar, 50 nm; shade-height scale, 0–2.5 nm. E and F, frequency distributions of molecular volumes of  $\alpha\beta\gamma$ -ENaC particles that were decorated by two anti-His<sub>6</sub> (E) or anti-V5 (F) antibodies. The curves indicate the fitted Gaussian functions. The means of the distribution are indicated. Note the absence of the lowest volume peak seen in Fig. 3, D–F, and Fig. 4C.

again suggested a channel stoichiometry of  $\alpha_2\beta\gamma$ . The behavior of  $\alpha\beta\gamma$ -ENaC on sucrose density gradients also suggested that the channel assembles as a tetramer (8), and the same conclusion was reached for the homologous homomeric FMRF-amide-gated sodium channel on the basis of chemical cross-linking and density gradient centrifugation (33).

Of all the methods used to date to determine the subunit stoichiometry of ENaC, ours is the most direct, in that we are actually visualizing individual antibody-decorated channels. Importantly, trimer superassembly could account for some of the conflicting results in the above studies, for example with respect to the detection of cross-linked products on gels and the behavior of ENaC on sucrose density gradients, where it has been reported to migrate either as tetramers or nonamers. Variations in protocol (e.g. 10, 11) could leave the complexes either intact with nine subunits or disassembled into three individual trimers, and it would be difficult to discriminate between trim-

ers and tetramers using these approaches. The effects of functional mutants and the behavior of subunit concatemers become difficult to interpret in the context of a large multipored structure, especially given reports of a functional interaction between the pores. A potential hazard of subunit concatenation is the possibility that not all subunits in the concatemer will participate in the formation of the complex, leading to erroneous results. For example, either  $\alpha_4\text{-}\beta_2$  or  $\beta_2\text{-}\alpha_4$  nicotinic acetylcholine receptor subunit dimers were unexpectedly found to form functional receptors (34). It was shown that dimers could be incorporated into two separate pentamers, leading to a receptor dimer held together by the linker. In another study, a functional P2X2 receptor was produced by expression of a concatenated subunit dimer (35), which is difficult to explain as we now know that the receptor is a trimer (15). Although the nicotinic acetylcholine receptor and P2X2 have only a single pore, the additional complexity we have shown here demonstrates that neither functional assessments nor concatemers are appropriate methods for determining ENaC subunit stoichiometry.

A number of further questions stem from our results. The state of functional ENaC in the membrane is unclear; for instance it is not known whether the trimer-of-trimers arrangement is stable or whether there is a dynamic relationship between single trimers and trimers-of-trimers. If the latter, then the possibility arises that the assembly state of ENaC can be modulated either physiologically or pharmacologically. It is also possible that there are functional implications of the different assembly states and that other proteins might form supercomplexes with ENaC in the plane of the membrane. Our AFM-based approach might help to shed light on some of these questions.

*Acknowledgments*—The expert technical assistance of Sonja Mayer and Ralf Rinke is gratefully acknowledged.

## REFERENCES

- Kellenberger, S., and Schild, L. (2002) *Physiol. Rev.* **82**, 735–767
- Loffing, J., and Korbmacher, C. (2009) *Pflügers Arch.* **458**, 111–135
- Canessa, C. M., Horisberger, J. D., and Rossier, B. C. (1993) *Nature* **361**, 467–470
- Canessa, C. M., Schild, L., Buell, G., Thorens, B., Gautschi, I., Horisberger, J. D., and Rossier, B. C. (1994) *Nature* **367**, 463–467
- Waldmann, R., Champigny, G., Bassilana, F., Voilley, N., and Lazdunski, M. (1995) *J. Biol. Chem.* **270**, 27411–27414
- Haerteis, S., Krueger, B., Korbmacher, C., and Rauh, R. (2009) *J. Biol. Chem.* **284**, 29024–29040
- Firsov, D., Gautschi, I., Merrill, A. M., Rossier, B. C., and Schild, L. (1998) *EMBO J.* **17**, 344–352
- Dijkink, L., Hartog, A., van Os, C. H., and Bindels, R. J. M. (2002) *Pflügers Arch.* **444**, 549–555
- Anantharam, A., and Palmer, L. G. (2007) *J. Gen. Physiol.* **130**, 55–70
- Snyder, P. M., Cheng, C., Prince, L. S., Rogers, J. C., and Welsh, M. J. (1998) *J. Biol. Chem.* **273**, 681–684
- Eskandari, S., Snyder, P. M., Kreman, M., Zampighi, G. A., Welsh, M. J., and Wright, E. M. (1999) *J. Biol. Chem.* **274**, 27281–27286
- Jasti, J., Furukawa, H., Gonzales, E. B., and Gouaux, E. (2007) *Nature* **449**, 316–323
- Stockand, J. D., Staruschenko, A., Pochynyuk, O., Booth, R. E., and Silverthorn, D. U. (2008) *IUBMB Life* **60**, 620–628
- Barrera, N. P., Henderson, R. M., and Edwardson, J. M. (2008) *Pflügers*

- Arch.* **456**, 199–209
15. Barrera, N. P., Ormond, S. J., Henderson, R. M., Murrell-Lagnado, R. D., and Edwardson, J. M. (2005) *J. Biol. Chem.* **280**, 10759–10765
  16. Kobori, T., Smith, G. D., Sandford, R., and Edwardson, J. M. (2009) *J. Biol. Chem.* **284**, 35507–35513
  17. Rauh, R., Diakov, A., Tzschoppe, A., Korbmacher, J., Azad, A. K., Cuppens, H., Cassiman, J. J., Dötsch, J., Sticht, H., and Korbmacher, C. (2010) *J. Physiol.* **588**, 1211–1225
  18. Diakov, A., and Korbmacher, C. (2004) *J. Biol. Chem.* **279**, 38134–38142
  19. Diakov, A., Bera, K., Mokrushina, M., Krueger, B., and Korbmacher, C. (2008) *J. Physiol.* **586**, 4587–4608
  20. Krueger, B., Haerteis, S., Yang, L., Hartner, A., Rauh, R., Korbmacher, C., and Diakov, A. (2009) *Cell Physiol. Biochem.* **24**, 605–618
  21. Korbmacher, C., Volk, T., Segal, A. S., Boulpaep, E. L., and Frömter, E. (1995) *J. Membr. Biol.* **146**, 29–45
  22. Schneider, S. W., Lärmer, J., Henderson, R. M., and Oberleithner, H. (1998) *Pflügers Arch.* **435**, 362–367
  23. Neaves, K. J., Cooper, L. P., White, J. H., Carnally, S. M., Dryden, D. T., Edwardson, J. M., and Henderson, R. M. (2009) *Nucleic Acids Res.* **37**, 2053–2063
  24. Scott, D. W. (1979) *Biometrika* **66**, 605–610
  25. Welch, B. L. (1947) *Biometrika* **34**, 28–35
  26. Huber, R., Krueger, B., Diakov, A., Korbmacher, J., Haerteis, S., Einsiedel, J., Gmeiner, P., Azad, A. K., Cuppens, H., Cassiman, J. J., Korbmacher, C., and Rauh, R. (2010) *Cell Physiol. Biochem.* **25**, 145–158
  27. Rossier, B. C., and Stutts, M. J. (2009) *Annu. Rev. Physiol.* **71**, 361–379
  28. Collier, D. M., and Snyder, P. M. (2011) *J. Biol. Chem.* **286**, 6027–6032
  29. Carnally, S. M., Dev, H. S., Stewart, A. P., Barrera, N. P., Van Bemmelen, M. X., Schild, L., Henderson, R. M., and Edwardson, J. M. (2008) *Biochem. Biophys. Res. Commun.* **372**, 752–755
  30. Carnally, S. M., Johannessen, M., Henderson, R. M., Jackson, M. B., and Edwardson, J. M. (2010) *Biophys. J.* **98**, 1182–1191
  31. Staruschenko, A., Medina, J. L., Patel, P., Shapiro, M. S., Booth, R. E., and Stockand, J. D. (2004) *J. Biol. Chem.* **279**, 27729–27734
  32. Ismailov, I. I., Awayda, M. S., Berdiev, B. K., Bubien, J. K., Lucas, J. E., Fuller, C. M., and Benos, D. J. (1996) *J. Biol. Chem.* **271**, 807–816
  33. Coscoy, S., Languaglia, E., Lazdunski, M., and Barbry, P. (1998) *J. Biol. Chem.* **273**, 8317–8322
  34. Zhou, Y., Nelson, M. E., Kuryatov, A., Choi, C., Cooper, J., and Lindstrom, J. (2003) *J. Neurosci.* **23**, 9004–9015
  35. Newbolt, A., Stoop, R., Virginio, C., Surprenant, A., North, R. A., Buell, G., and Rassendren, F. (1998) *J. Biol. Chem.* **273**, 15177–15182